Microstructure and viscosity of semi-solid mixtures

2000 J. Phys.: Condens. Matter 12 2567

(http://iopscience.iop.org/0953-8984/12/12/301)

J. Phys.: Condens. Matter **12** (2000) 2567–2577. Printed in the UK PII: S0953-8984(00)08027-9

Microstructure and viscosity of semi-solid mixtures

J C Barbé†, M Perez‡ and M Papoular†§

† Laboratoire de Solidification et de ses Procédés, DTA/SPCM, CEA Grenoble, 17 rue des Martyrs, 38 054 Grenoble Cédex 9, France
‡ Laboratoire Génie Physique et Mécanique des Matériaux, UPRESA CNRS 5010, BP 46, 38 402 Saint Martin d'Hères Cédex, France
§ Centre de Recherche sur les Très Basses Températures, CNRS, BP 166, 38 042 Grenoble Cédex, France

E-mail: barbe@chartreuse.cea.fr

Received 22 September 1999

Abstract. The semi-solid state of metallic alloys is characterized by the coexistence of solid and liquid phases at thermal equilibrium. The rheology of such diphasic materials not only depends on the solid fraction, but also is highly correlated with the degree of aggregation of the solid particles. The viscosity η of a diphasic (30% and 40% solid fractions) Ag–Cu alloy was measured using a contactless method: at 923 °C, we get $\eta = (2 \pm 1) \times 10^3$ Pa s for a solid fraction of 30% and $\eta = (2 \pm 1) \times 10^4$ Pa s for a solid fraction of 40%. The solid, copper-rich phase, is dispersed into globules of about 50 μm in size. The large value of η suggests that these particles form a random interconnected network. This type of microstructure is likely to give rise to the thixotropic rheological properties of many semi-solid materials. The structure and therefore the viscosity are sensitive to the applied shear rate $\dot{\gamma}$. Two distinct regimes of aggregation, depending on the actual value of the shear rate, are discussed: 'compact clusters' versus 'random network'. We calculate the characteristic size of the compact clusters and discuss the parameters governing the state of aggregation.

1. The semi-solid state

When an alloy is brought between the liquidus and solidus and reaches approximate thermal equilibrium, it is of course in a diphasic state with some solid fraction ϕ_s determined by the lever rule. This solid fraction may be more or less finely dispersed depending on previous mechanical stirring and heat treatment. This is the semi-solid state. A simple example is provided by the mushy zone in solidification processes: a highly viscous mixture of more or less broken dendrites coexisting with the interdendritic melt.

Semi-solids lend themselves to various important practical applications, e.g.

(i) the development, after complete solidification, of appropriate microstructures leading to specific material properties; and
(ii) the casting of thixotropic slurries (rheocasting) improving the forming processes for metals [1] ('thixotropy' is non-linear and non-reversible shear thinning, due to shear-induced structural modifications).

Clearly, the physical properties—and the physics—of semi-solids are related to those of suspensions and of granular media. The viscosity, η, for instance is expected to diverge at, or near, random loose packing and/or the onset of rigidity percolation [2]. Near walls, plug flows [3] or slip bands [4] may appear, resulting in lower apparent viscosity.

0953-8984/00/122567+11$30.00

Semi-solids are special, however, in that the liquid and solid phases are chemically related: strictly, at equilibrium, their chemical potentials are equal, and one phase can locally melt, or freeze, into the other. This will lead to specific microscopic modes of aggregation (agglomeration) of solid particles [1], related to liquid-phase sintering, and different from sticking mechanisms in, say, colloidal suspensions. In both cases however, aggregation will generally result in divergence (or at least rapid increase) of the viscosity, at some volume solid fraction value Φ_g^s. The state of aggregation itself, i.e. the semi-solid microstructure, is difficult to predict and describe: the number density and compactness of the clusters will depend on solid fraction, shear strain, temperature, and size and shape of individual solid particles.

In this paper we are interested in the viscosity of metallic alloys in the semi-solid state as related to their microstructure: the central question is that of whether they have suspension-like behaviour described by hard-core models (see e.g. [5]) or a more complex behaviour affected by the interaction between the particles. Experimental results obtained on semi-solid alloys exhibit large viscosities at low shear rates, even at relatively low solid fractions (see for instance reference [6]). As a consequence, interactions between solid particles have to be taken into account. Two limiting cases are presented and discussed: (i) formation of 'compact' clusters; and (ii) a random loose network. The aim of this paper is to determine the physical parameters controlling the steady microstructure under shear.

In section 2, we describe the development of a silver–copper semi-solid sample, and report viscosity measurements on that sample. In section 3, we calculate the limiting size, under external shear, of compact globular clusters. Two basic cluster-growth scenarios are considered in section 4, resulting in compact or open, colloid-like clusters.

2. Elaboration of an Ag–Cu semi-solid sample and contactless viscosity measurements

Our gas–film levitation viscosimeter has been described and demonstrated in detail elsewhere [7, 8]. Its main advantages are:

(i) no walls, and very reduced heterogeneous nucleation, which allows measurements on substantially supercooled liquids;
(ii) a large range of accessible temperatures (20–2500 °C) and viscosities (10^{-3}–10^5 Pa s);
(iii) relatively modest shear rates ($\leqslant 1\ s^{-1}$).

Our new method is based on the hydrodynamics of a deformed viscous drop [9]. Depending on the characteristic viscosities, the set-up can be operated in the oscillatory regime [8, 10] or in the aperiodic regime [7]. When the radius of the drop R is larger than the critical radius ($R_c = \eta^2/(\sigma\rho)$, η viscosity, σ surface tension, and ρ density), the regime will be oscillating. When the drop radius is smaller than R_c, the regime will be aperiodic with a characteristic time constant for deformation mode ℓ [9] of

$$\tau_\ell = \frac{2(2\ell^2 + 4\ell + 3)}{\ell(\ell + 2)(2\ell + 1)} \frac{\eta R}{\sigma} \tag{1}$$

where ℓ is the deformation mode index ($\ell \geqslant 2$). The relaxation curve is then an exponential with the characteristic time constant τ_ℓ. Here we are only interested in the viscous case and the $\ell = 2$ mode (the drop initially compressed along the vertical axis). So, the characteristic time constant of the aperiodic relaxation, after imposed deformation, depends linearly on the viscosity. We have

$$\eta = \frac{40}{38} \frac{\sigma}{R} \tau_2. \tag{2}$$

The method has been successfully tested [7] on a silicate glass: 'AR-Glas', and oxide glass mixtures (SiO_2–Na_2O–B_2O_3) between 800 and 1200 °C for viscosities ranging between 10^2 and 10^5 Pa s.

Our silver–copper samples, drops with equatorial radius $R \approx 4$ mm and composition 28.8 wt% silver, corresponding to a solid fraction $\Phi_s = 30\%$ at 923 °C (a temperature corresponding to liquid–solid iso-density in order to avoid sedimentation effects), were thermomechanically pre-treated in order to obtain a reproducible globularized microstructure with globule size of order 50 μm (see figure 1(a)). Here are the successive steps of this thermomechanical treatment:

- First, the sample is developed in a graphite crucible and solidified by quenching (100 °C per minute). The microstructure is then dendritic with Cu-rich dendrites.
- Second, the ingot is rolled to a high rolling strain (more than 50%).
- The main consequence of this mechanical preparation is to induce re-crystallization leading to the formation of globular microstructure (characteristic radius 50 μm) during the last step of the treatment: partial remelting at 923 °C.

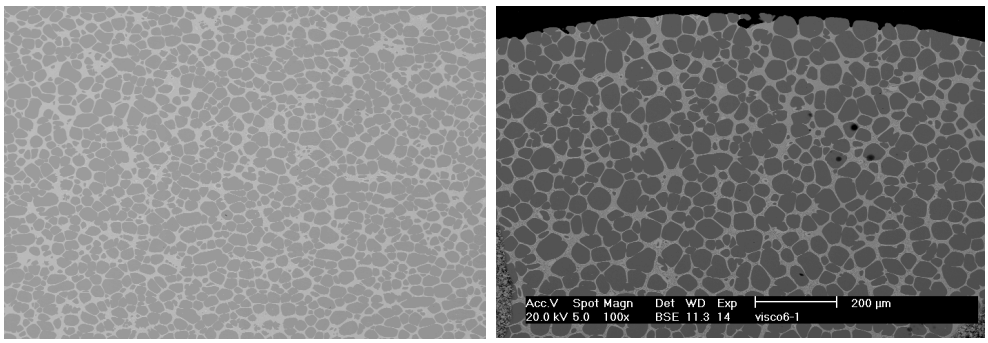

Figure 1. Globularized Cu–28.8 wt% Ag after mechanical treatment and quenching: (a) oil quenching (magnification ×80); (b) after completing the viscosity measurement and air quenching (magnification ×100). Note that quenching alters the apparent solid fraction.

Remarks

(a) In figure 1(a), the sample was quenched in oil with a cooling rate of order 500 °C min^{-1} after partial remelting at 923 °C for 15 minutes, so we can consider the recorded characteristic size in the picture—about 100 μm—to represent the actual solid particle size at 923 °C. Figure 1(b) shows the microstructure after completing the viscosity measurement: the characteristic size is of the same order as in figure 1(a), so we conclude that there is no significant change in the microstructure of our sample over the duration of the viscosity measurement (a few minutes). This observation leads us to make the further (and stronger) assumption that, over this same measurement duration, the particle interconnectivity itself (see below, at the end of this section) does not change, which allows us to disregard any rheofluidization effects due to the measurement itself (at least as long as the initial deformation remains relatively small).

(b) The micrographies represent two-dimensional sections of the sample and so, at the moment, we are not able to correlate the apparent agglomeration with the actual agglomeration of the particles in three dimensions.

We take the characteristic shear rate to be

$$\dot{\gamma} = \frac{1}{R}\frac{\Delta\delta}{\tau}$$

where R is the drop radius, τ is the relaxation time extracted from figure 2, and $\Delta\delta$ is the effective range of drop-deformation relaxation (vertical axis in figure 2). We thus estimate: $\dot{\gamma} \approx 10^{-2}$ s^{-1}. The temperature inhomogeneity is less than a few degrees between the top (north pole) and the centre of the drop. The microstructure of our sample after the viscosity measurement is presented in figure 1(b).

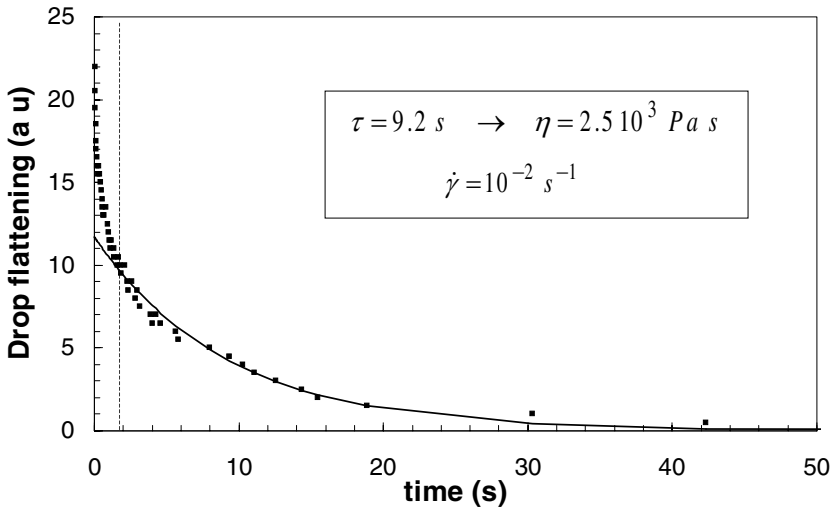

Figure 2. A typical relaxation curve for Cu–28.8 wt% Ag in the semi-solid state. Temperature of the experiment: 923 °C; volumic solid fraction: 30%. The useful part of the curve is beyond the vertical dotted line (see the text following equation (3)).

The extracted relaxation time constant is $\tau \approx 10$ s, which yields via equation (2) a viscosity (averaged over five independent measurements) of

$$\eta = (2 \pm 1) \times 10^3 \text{ Pa s.} \tag{3}$$

The 50% uncertainty is due to the actual shape of the relaxation curve as shown in figure 2. At first ($\approx$1 s) the relaxation is extremely fast (this is a purely mechanical effect associated with the rapid withdrawal of a liquid-rich zone at the pole of the drop on removing vertical compression).

We have also performed viscosity measurements at solid fractions of 20 and 40%. At $\Phi_s = 40\%$, we get: $\eta \approx 2 \times 10^4$ Pa s ($\dot{\gamma} \approx 10^{-3}$ s^{-1}; of course, with our technique, $\dot{\gamma}$ cannot be independently varied as it could, e.g., in a Couette rheometer). At $\Phi_s = 20\%$, the relaxation is too fast and we are unable to measure any viscosity lower than 10 Pa s; this means that the microstructure is much less interconnected and the individual particles more independent of one another (see below).

We note that, at $\Phi_s = 30\%$ and $\dot{\gamma} = 10^{-2}$ s^{-1}, previous viscosity measurements on Sn–15 wt% Pb [6] yield $\eta \approx 5 \times 10^4$ Pa s—that is, more than an order of magnitude higher

than our result, equation (3). This is, in all probability, due to the different mechanical properties of the solid phase, resulting in easier brittle rupture in Ag–Cu, and therefore in weaker particle interconnectivity (see section 3).

The present gas–film levitation viscosity measurements, which we believe are the first of this kind, on the viscosity of a metallic alloy in the semi-solid state, allow us to make the following statements. This dramatic increase in viscosity, due to particle aggregation, is well known in colloidal suspensions [21, 23] as well as in oxide and metallic melts [25]. The elemental structural units (globules) are not like independent solid particles in a suspension. Rather, they are massively aggregated and this leads to the very high viscosity given by equation (3): η is about five orders of magnitude larger than what would be obtained by calculation for a simple suspension with the same solid fraction. In the following sections, we shall discuss, phenomenologically, simple agglomeration mechanisms which might explain these wide structural and rheological gaps.

3. Shear-limited aggregation: limiting size of a globular cluster

In this section we shall give an evaluation of the maximum size of a cluster of solid particles when agglomeration is counteracted by shear. We shall make a number of simplifying, but not necessarily very restrictive, assumptions:

(i) The individual solid particles are, as explained earlier, preformed globular crystals: we take them to be spherical and monodispersed.
(ii) When subjected to a modest shear stress, these particles will agglomerate as we shall explain next. We assume that there is enough time for structural rearrangements to result in clusters which we again take to be spherical and monodispersed, though not in general of good crystalline quality.
(iii) These globular lumps grow over time by shear-induced cluster–cluster aggregation until they reach their maximum size $R_{max} = f(\dot{\gamma})$ compatible with the shear-rate field $\dot{\gamma}$ (which we take to be uniform on the scale of R_{max}; this assumption is crude but not critical). Any cluster larger than R_{max} would be torn apart by the shear stress.

Two spherical objects with radius R, directed towards one another in a shear flow with shear rate $\dot{\gamma}$, will meet and roll over one another in a time τ_0 given, on average, by (see e.g. reference [11])

$$\tau_0 = 2.5\dot{\gamma}^{-1}. \tag{4}$$

For modest shear rates, τ_0 is relatively long, which provides the two spheres (that are in close contact for the time τ_0) with the opportunity to sample favourable relative crystallographic orientations over their surfaces. We then assume that during the time τ_0 they will form fairly low-energy grain boundaries: these will grow rapidly, leading to a new generation of fewer but larger clusters. (We note, however, that, during this coarsening process, structural rearrangements over larger and larger distances progressively become less efficient at maintaining the spherical cluster shape and, hence, coarsening the self-similarity.)

We now use a result that was derived in reference [12] concerning the growth rate of a 'neck' between two solid spherical particles with equal radii R; see figure 3. If x is the neck radius (the radius of the grain boundary circular disc), then at time t after a particle encounter, x is given by

$$t = R^3\left[\frac{m(C_L - C_S)}{4D}\frac{\Delta S^*}{\sigma_{SL}}\right] f\left(\frac{x}{R}\right) = R^3 A f\left(\frac{x}{R}\right) \tag{5}$$

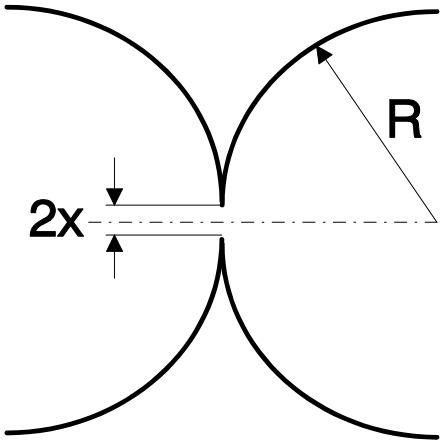

Figure 3. Neck growth between two solid particles.

where $f(x/R) \approx (x/R)^5/5$ as long as $x/R \ll 1$, and m is the liquidus slope, C_L and C_S are the solute concentrations at the liquidus and solidus, D is the solute diffusivity, σ_{SL} is the solid–liquid surface tension, and ΔS^* is a weighted entropy change per unit volume as defined in [12]. In fact, neck growth may start early or late on the scale of the 'mating' time τ_0 (equation (4)), depending on whether or not favourable crystallographic orientations are found for which the grain boundary surface energy σ_b is substantially smaller than σ_{SL}. However, if it starts too late, the neck will be fragile and the two 'particles' (clusters) will break apart. In practice therefore, the scale for the relevant time of neck growth is given by τ_0. If the corresponding neck size x, given by equation (5), is large enough to withstand hydrodynamic shear stress, aggregation will succeed and lead to cluster coarsening. It is then clear that the limiting cluster size R_{max}, for a shear rate $\dot{\gamma}$, is given (together with neck size x_0 corresponding to that 'maximal' cluster) by the following two coupled equations:

$$\tau = 2.5\dot{\gamma}^{-1} = R_{max}^3 A \frac{1}{5}\left(\frac{x_0}{R_{max}}\right)^5 \tag{6}$$

$$\frac{1}{2}MV^2 = \frac{1}{2}\rho\frac{4}{3}\pi R^3(\dot{\gamma}R_{max})^2 = \pi x_0^2\,\Delta\sigma. \tag{7}$$

In the latter equation, we equate the differential kinetic energy available for disagglomeration to the rupture energy of the virtual cluster that would be formed by aggregation of the two 'colliding' spherical objects of radius R_{max} (see point (iii) in the following discussion). M and ρ are the effective mass and the density of these objects (taking backflow into account) and $V \approx \dot{\gamma}R$ is their relative velocity in the local shear field. $\Delta\sigma = 2\sigma_{SL} - \sigma_b$ is the energy barrier per unit grain boundary area for boundary rupture—that is, formation of two solid–liquid interfaces replacing the solid–solid interface between two particles.

Combination of equation (6) and equation (7) leads to the following maximum values for x and R:

$$R_{max} = \left(\frac{25}{2A}\right)^{2/21}\dot{\gamma}^{-4/7}\left(\frac{3\,\Delta\sigma}{2\rho}\right)^{5/21} \tag{8}$$

$$x_0 = \left(\frac{25}{2A}\right)^{5/21}\dot{\gamma}^{-9/21}\left(\frac{3\,\Delta\sigma}{2\rho}\right)^{2/21}. \tag{9}$$

R_{max} decreases with shear rate roughly as $\dot{\gamma}^{-1/2}$ and varies with an extremely weak dependence on the thermodynamic parameters: in particular, R_{max} depends on $\Delta\sigma$ with an exponent $-5/21 \approx -1/4$; the numerical prefactor is such that, for a (rather strong) shear rate of $\dot{\gamma} = 10^3$ s^{-1}, R_{max} and x_0 are respectively close to 100 μm and 10 μm. It is interesting to note at this point that globular microstructures in a number of different metallic alloys have characteristic sizes of order 100 μm for shear rates of several hundred s^{-1} (see e.g. references [6, 13]).

3.1. Discussion

(i) Equation (8) could be seen as a lower limit for R_{max}, given by the energetic cost of the boundary rupture of two clusters. An upper limit could be estimated as the energy of the fragile rupture of the neck between two particles after plastic deformation, giving a value a few times larger. The scenario usually considered [14] for dendritic-arm fracture consists in a localized plastification leading to the formation of sub-grain boundaries which are then wetted by the liquid.

(ii) Equations (8) and (9) provide us with two pieces of information: R_{max} and x_0, the characteristic neck size just before the disagglomeration threshold is reached.

On the other hand, at early stages (cluster 'generations') of the agglomeration process, R is smaller (or much smaller if the initial particles are themselves small) than R_{max}. Thus, it follows from equation (5) that the relative neck size is larger for smaller clusters: at this stage sintering is quite efficient and the clusters are robust (albeit polycrystalline). Whereas the neck growth is diffusion limited and follows a Gibbs–Thomson-like kinetic form (see equation (5)), the cluster growth itself is governed by the collision frequency as long as $R \leqslant R_{max}$, leading to an exponential growth (see section 4): thus cluster growth is much faster than classical, diffusion-limited coalescence, whereby $R \approx t^{1/3}$ just as for Lifshitz–Slyozov coarsening [15].

(iii) It must be stressed, however, that the results above (and equation (4) in particular) were derived under the binary-collision assumption. In fact, since we are interested in practice in solid fractions that are no less than 20%, multi-particle collisions are frequent, with two antagonistic consequences: (a) a tendency for faster growth; and (b) less robust sintering, since the crystallographic orientation sampling, as mentioned just after equation (4), will be hindered by hard-core effects. From the discussion in (ii), we expect trend (a) to dominate for smaller clusters. As growth proceeds, the actual clusters become less and less homogeneously compact, and change from pseudo-spherical to dumb-bell shaped. Note that this same argument provides us with a semi-quantitative justification for our energetic balance (equation (7)): due to particle crowding (already occurring at intermediate solid fractions), the available kinetic energy is readily converted into disagglomeration energy ($\pi x_0^2\,\Delta\sigma$) when $R \approx R_{max}$.

(iv) A comparison is made in table 1 between our equation (8) and experimental 2D micrographies for Al–Zn–Mg [13] and Sn–Pb [12], and 3D micrographies for Al–Si [20]. R_{max} is found to be of the correct order of magnitude for these alloys at high shear rate ($\dot{\gamma} = 100$–1000 s^{-1}). For Sn–Pb no micrographies are available in the literature. Equation (8) is obviously not meant to describe the microstructure of our Ag–Cu levitated droplet for a $\dot{\gamma} = 10^{-2}$ s^{-1} shear rate: in our experiment on Ag–Cu drops, as described in section 2, the individual solid globules are rather large ($R \approx 50$ μm), and are probably already interconnected from the start due to the thermomechanical history of the sample. In fact, we consider a random-network scenario to be the only way to explain the result reported in section 2: a semi-solid whose viscosity is at least five orders of magnitude

Table 1. Thermodynamical parameters and final sizes of clusters: comparison between results from calculations (equation (8)) and micrographies for Al–6Zn–3Mg [13], Al–6.5 wt% Si [20], and Sn–15 wt% Pb [12].

	Al–6Zn–3Mg	Al–6.5 wt% Si	Sn–15 wt% Pb	Cu–28.8 wt% Ag
m (K/%)	2.9 [16]	6.7 [16]	3.3 [17]	3.3 [16]
$C_L - C_S$ (wt% K^{-1})	12 [16]	5.5 [16]	23 [17]	28.4 [16]
D (10^{-9} m^2 s^{-1})	6.2 [18]	5 [18]	4 [18]	4 [18]
σ_{SL} (J m^{-2})	0.16 [17]	0.17 [17]	0.13 [19]	0.23 [19]
ΔS^* (10^5 J K^{-1} m^{-3})	6.8 [17]	8.6 [17]	17 [17]	1.7 [17]
ρ (kg m^{-3})	2580 [16]	2360 [16]	7500 [16]	8500 [16]
$\dot{\gamma}$ (s^{-1})	610 [13]	900 [20]	100 [6]	100[a]
$\Delta\sigma$ (J m^{-2})	0.33 [17]	0.34 [17]	0.26 [19]	0.43 [19]
Apparent agglomerate radius (μm)	100–300 [13]	200–400 [20]	—	—
R_{max} (μm) (equation (8))	130	100	220	320

[a] This value of the shear rate $\dot{\gamma}$ is given simply for comparison, and does not correspond to any actual measurement.

larger than that of a typical liquid metal ($\leqslant 10^{-2}$ Pa s), at a solid fraction of 'only' 30%. We are currently preparing quenching and visualization procedures, aiming to display this interconnected microstructure. In fact, as we have already pointed out, when clusters grow to larger sizes, compactifying rearrangements require longer times τ_r. When τ_r becomes comparable to, or larger than, the cluster–cluster sticking collision time, τ_{coll}, an interconnected random network necessarily sets in—with a concomitant rapid increase in viscosity (gelation). This point is central; although calculating τ_r is no easy task, it is clear that eventually the gel transition will put an end to the cluster-growth mechanism discussed above: instead of equation (8), R_{max}, or rather, in that case, the characteristic size of the microstructure will level off as shear rate decreases (except when $\Phi_s \ll 1$), at a value of order 100 μm, in agreement with our Ag–Cu micrographies. The gel point will occur at larger (lower) solid fraction for smaller (larger) individual solid particles. For example, in a refined (finely dispersed) aluminium alloy, each cluster 'blob' is more compact; it is made up of a larger number of single particles, and gelation will accordingly start at larger solid fraction. We now consider this point in somewhat more detail.

4. Fractal versus compact clusters

The viscosity measurements reported in section 2 gave evidence for strong interactions between individual solid particles. The micrographies presented in figure 1 led us to make the assumption of a fractal-like structure: gelation would then occur when a fractal cluster manages to reach the size of the sample.

For individual spherical particles of size a and number density n, we may write the volume density, i.e. solid fraction, as

$$\Phi_s = \frac{4}{3}\pi a^3 n. \tag{10}$$

The linear size of a cluster of fractal dimension d containing N particles is

$$R = aN^{1/d}. \tag{11}$$

For compact clusters, d is the space dimension: $d = 3$; for fractal clusters growing by cluster diffusion-limited aggregation, d lies between 1.7 and 1.9 for colloids (see for example

reference [21]). The number density and volume fraction for such clusters are n/N and $(n/N)(4/3)\pi a^3 N^{3/d} = \Phi_s N^{(3-d)/d}$, respectively. For compact clusters we naturally find the volume fraction to be just Φ_s whatever the cluster size; for fractal clusters where $d < 3$, gel will start forming when the cluster fraction reaches unity—that is to say, when percolation occurs. We now examine the rate at which cluster growth proceeds, before R_{max} (see section 3) or the gelation onset is reached. In shear flow, the classical Smoluchowski cluster–cluster collision frequency (again for spherical objects) is given by: $(8/\pi)\Phi_s N^{(3-d)/d}\dot{\gamma}$. Recall that, for objects larger than a few micrometres, Brownian motion can be neglected in practice and collisions are essentially shear induced. The rate of cluster-size increase is therefore given by

$$\dot{N} = N\frac{8}{\pi}\Phi_s N^{(3-d)/d}\dot{\gamma} \approx 2.5\dot{\gamma}\Phi_s N^{3/d}. \tag{12}$$

For compact clusters ($d = 3$), the growth is therefore exponential with an exponent proportional to the product $\dot{\gamma}\Phi_s$; but recall that it saturates at R_{max}. For fractal clusters ($d \leqslant 3$), equation (12) once integrated transforms into

$$N = \left[\text{constant} - 2.5\left(\frac{3-d}{d}\right)(\dot{\gamma}\Phi_s)t\right]^{-d/(3-d)} \tag{13}$$

with saturation for the cluster volume fraction $\approx$1, and the constant of order 1 (since $N = 1$ at $t = 0$).

Exact self-similarity, as associated with fractals, is not postulated here, but an effective exponent d as defined in equation (11) will still characterize the compactness of the network, whether truly fractal or not. Depending on $\dot{\gamma}$ and Φ_s, d can range between 1.7 (colloidal fractals resulting from diffusion-limited aggregation) and 3 (compact clusters). Gelation, or percolation of the fractal-like network, must then be considered in the plane (Φ_s, $\dot{\gamma}$). At a given solid fraction, gelation will occur as $\dot{\gamma}$ decreases whereas, at a given shear rate, the percolation of a three-dimensional network (gelation) will begin as Φ_s increases.

When gelation occurs at a large solid fraction ($\Phi_s^g \geqslant 50\%$) at a given shear rate, we may consider in practice that the viscosity increase at $\Phi_s \leqslant \Phi_g^s$ is governed by the small available free volume between the blobs and, therefore, by Krieger's empirical law for dense suspensions [5]:

$$\eta = \eta_0\left(1 - \frac{\Phi_s}{\Phi_s^g}\right)^{-k} \qquad k \approx 2.5\Phi_s^g. \tag{14}$$

In that regime, as we have also suggested elsewhere [22], the shear-rate onset for shear thinning should decrease, as $\Phi_s \to \Phi_s^g$, roughly as τ_β^{-1}, an inverse β-relaxation time in the suspension. We will not spend time here on the difficult question of the history-dependent modifications in structure and viscosity (hysteresis in shear strain as a function of shear stress) that may be found in thixotropic materials. We simply note that jumps in applied shear [12] may lead to some understanding of agglomeration and disagglomeration processes.

Conversely, when gelation occurs at intermediate solid fractions ($\Phi_s^g \leqslant 30\%$), because τ_r rapidly surpasses τ_{coll} as R increases, we expect the clusters to be 'open' rather than compact, and the microstructure to be 'branched ' or colloid-like rather than globular. Viscosity should then increase as $\Phi_s \to \Phi_s^g$ according to the percolation law [11]

$$\eta = \eta_0\left(1 - \frac{\Phi_s}{\Phi_s^g}\right)^{-s} \qquad s \approx 0.7 \text{ for colloids [21].} \tag{15}$$

In that case, Φ_s^g marks the earlier onset of an 'infinite' interconnected network of single solid particles throughout the sample. Of course, even above Φ_s^g, viscosity may be large but finite, owing to shear-induced defects: re-dissolved grain boundaries, acting as 'broken

bonds', will allow some creep motion. As shown in reference [13], the stable grain boundaries are those where intergrain relative crystallographic orientations are sufficiently energetically favourable that $\sigma_b < 2\sigma_{SL}$, where σ_b is the boundary energy and σ_{SL} the interfacial solid–liquid surface tension. In different physico-chemical contexts, these two asymptotic regimes (with material-dependent exponents k and s) may be found in silica gels or colloidal suspensions [21].

Remarks

(i) In equation (15), for globular non-compact clusters, the value of s is not known but is probably close to 2.5.

(ii) In equations (14) and (15), in order to take into account rheofluidization, Φ_s has to be taken as an effective volume fraction (including some entrapped liquid) [23].

The fractal scenario is clearly a better fit to colloids. In diphasic alloys the compact, globular route probably provides a reasonable description of cluster growth as long as the cluster size R is substantially smaller than R_{max}, as we saw in section 3. But, when $R \approx R_{max}$—or when the shear rate ($\dot{\gamma}$) is relatively small, such that the 'equilibrium' R_{max} (equation (8)) would be too large for compactifying rearrangements to take place—then the late stages of growth would probably be characterized by a more 'open' microstructure, perhaps with some short filamentary or ribbon-like segments. The latter will, eventually, form an interconnected (if not truly fractal) random structure at the gel point. In the case of the Ag–Cu diphasic drops discussed in section 2, we believe that gelation occurs right away in view of the large size of the individual solid particles. These considerations will be developed at greater length in a separate publication [26].

5. Concluding remarks

This work on the semi-solid state is sketchy and deals only with quite limited aspects of the subject. Yet we feel that we have posed one central question: are there indeed two distinct regimes depending on the actual value of the volume solid fraction at the gel onset, Φ_s^g, with quite different microstructural and rheological properties?

To try and get a more complete answer to that question, we need not only further viscosity measurements, but also microstructural investigation techniques. One of these is of course classical 2D micrography, but, as stressed e.g. in reference [20], such micrography does not always adequately reflect the reality of 3D aggregates or networks. One new observational technique may be fruitful: synchrotron-radiation microtomography allowing 3D investigation by means of phase contrast of a relatively large part of the sample (around 1 mm^3) with a resolution of a few micrometres [24].

In the compact-cluster scenario, we have evaluated the maximum cluster size R_{max} as a function of shear rate $\dot{\gamma}$, at high shear rate. This result is in fair agreement with micrographies available in the literature (see table 1). In the random-network scenario, our viscosity measurement on Ag–Cu at $\Phi_s = 30\%$ and $\dot{\gamma} \approx 10^{-2}$ s^{-1} yields an estimated viscosity of $\eta = 2 \times 10^3$ Pa s. Clearly, the size and the shape of individual solid particles will affect the crossover range, in Φ_s and $\dot{\gamma}$, between the compact and open-structure regimes. But, in both regimes, gel onset and steeply rising viscosity will occur as the solid fraction Φ_s increases and the shear rate $\dot{\gamma}$ decreases.

Acknowledgments

We are grateful to Y Bréchet, D Camel, C Martin and L Salvo for useful discussions. This work was partly funded by Electricité De France (EDF) and CEA.

References

[1] Suéry M, Martin C L and Salvo L 1996 *Proc. 4th Int. Conf. on Semi-Solid Processing of Alloys and Composites (Sheffield)* ed D H Kirkwood and P Kapranos, p 21
[2] Onoda G Y and Liniger E G 1990 *Phys. Rev. Lett.* **64** 2727
[3] Nozières P and Quemada D 1986 *Europhys. Lett.* **2** 129
[4] Veje C T, Howell D W and Behringer R P 1999 *Phys. Rev.* E **59** 739
[5] Woods M E and Krieger I M 1970 *J. Colloid Interface Sci.* **34** 91
[6] Laxmanan V and Flemings M C 1980 *Metall. Trans.* A **11** 1927
[7] Barbé J C, Parayre C, Papoular M, Kernevez N and Daniel M 1998 *Int. J. Thermophys.* **20** 1071
[8] Perez M, Bréchet Y, Salvo L, Papoular M and Suéry M 1999 *Europhys. Lett.* **47** 189
[9] Chandrasekhar S 1990 *Hydrodynamic and Hydromagnetic Stability* (New York: Dover)
[10] Perez M, Papoular M, Bréchet Y, Salvo L and Suéry M 2000 *Phys. Rev.* E **61** at press
[11] de Gennes P G 1979 *J. Physique* **40** 783
[12] Martin C L, Kumar P and Brown S 1994 *Acta Metall. Mater.* **42** 3603
[13] Lee H L, Doherty R D, Feest E A and Titchmarsh J M 1980 *Solidification Technology in the Foundry and Cast House (Coventry)* (London: The Metals Society) p 119
[14] Flemings M C 1991 *Metall. Trans.* B **22** 269
[15] Siggia E D 1979 *Phys. Rev.* A **20** 595
[16] ASM Handbook Committee 1973 *Metals Handbook* vol 8 (Metals Park, OH: American Society for Metals)
[17] Gündüz M and Hunt J D 1985 *Acta Metall.* **33** 1651
[18] Roy A K and Chhabra R P 1988 *Metall. Trans.* A **19** 273
[19] Eustathopoulos N, Joud J C and Desré P 1974 *J. Chim. Physique* **71** 777
[20] Ito T, Flemings C and Cornie J A 1991 *Nature and Properties of Semi-Solid Materials* (Warrendale, PA: The Minerals, Metals and Materials Society)
[21] Poulain P, Bibette J and Weitz D A 1999 *Eur. Phys. J.* B **7** 277
[22] Papoular M 1999 *Phys. Rev.* E **60** 2408
[23] Quemada D 1998 *Eur. Phys. J.* A **1** 119
[24] Buffières J Y, Maire E, Cloetens P, Lormand G and Fougères R 1996 *Acta Mater.* **47** 1613
[25] Ramacciotti M 1999 Etude du comportement rhéologique de mélanges issus de l'interaction corium/béton *PhD Thesis* Université de Provence (Aix-Marseille I)
[26] Perez M, Barbé J C, Neda Z and Bréchet Y 2000 unpublished